High bandwidth back-scanning mirror for coherent chirped pulse lidar imaging

Andrew Oliver, Adam Eichhorn, Samantha Hampshire, David Dickensheets

Andrew D. Oliver, Adam X. Eichhorn, Samantha J. Hampshire, David L. Dickensheets, "High bandwidth back-scanning mirror for coherent chirped pulse lidar imaging," Proc. SPIE 12013, MOEMS and Miniaturized Systems XXI, 120130B (1 March 2022); doi: 10.1117/12.2610861

Event: SPIE OPTO, 2022, San Francisco, California, United States

High bandwidth back-scanning mirror for coherent chirped pulse lidar imaging

Andrew D. Oliver*[a] , Adam X. Eichhorn[ab] , Samantha J. Hampshire[a] and David L. Dickensheets[a]
[a]Montana State University, Bozeman, MT, USA; [b]Iowa State University, Ames, IA, USA
*andrew.oliver@montana.edu; phone 1 406 994 7915; fax 1 406 994-5958; https://ece.montana.edu/

ABSTRACT

This paper reports a secondary scan mirror for step-stare lidar applications that is single axis and operates in a non-resonant mode. The mirror has a resonant frequency of 61 kHz and a diameter of 2 mm with angular scan range equivalent to 10 resolvable spots at 780 nm. Hand calculations and finite element simulations showed good correlation with experimental results. The mirror, which is 300 μm thick, achieves torsional motion through electrostatic force electrodes placed 3 μm beneath it. Simulations and measurements suggest that static and dynamic mirror deformation remains below the diffraction limit.

Keywords: MEMS, back-scanning, mirror, coherent, lidar, step-stare

1. INTRODUCTION

This paper describers a secondary MEMS mirror for lidar applications that works with the primary mirror in a step-stare configuration. The secondary mirror counteracts the movement of the primary mirror and enables the primary mirror to move continuously while the secondary mirror keeps the beam stationary and on a target. The paper describes the motivation for the step-stare scheme, the design, finite element simulation, fabrication, and experimental results. Because of system requirements, the secondary mirror does not need to have a large angular deflection, just as large a bandwidth and as small a settling time as possible. This mirror is electrostatically actuated and has a resonant frequency of 61 kHz, a diameter of 2 mm, and scans a range equivalent to ten resolvable spots at a wavelength of 780 nm. The mirror is supported by two torsion springs that are 80 μm wide, 300 μm thick and 125 μm long.

2. MOTIVATION

Coherent detection lidar is extremely sensitive, so long as the reflected beam is properly matched to the mode that interferes with the local oscillator. When matching and coupling is poor, the detected signal strength drops sharply. One cause of mismatch and poor coupling is wavefront tilt error, which can occur when the scan mirror moves during the transmit pulse and the backscatter return. The problem is exacerbated for coherent lidar because the frequency-chirped pulse can be many tens or even hundreds of microseconds long, with the pulse length inversely proportional to the range resolution. Maximum sensitivity and range resolution are achieved by recording the full duration of the returned pulse echo.

Figure 1 is a plot of the point spread function (PSF) for a coherent interferometric receiver. It plots the normalized detected power as a function of beam scan angle. The parameters used in calculating Figure 1 are the same as used in reference 1: a beam waist located at the exit pupil, and a pupil radius equal to 1.2 times the $1/e^2$ intensity radius (beam waist radius)[1]. The point scatterer is located in the far field. For a scanned beam with a continuously changing beam angle, the detected pulse will be apodized in time as the finite width of the collimated beam (the PSF of Figure 1) moves across the scatterer. This reduces both signal strength and distance resolution.

With a different scanning pattern such as step-stare, the movement-induced apodization can be eliminated. In step-stare, the scanner is synchronized with the laser pulse. It is advanced to a new pointing angle (step) and the angle is held constant during the transmit pulse and backscatter return (stare). Large mirrors, however, such as those found in long range lidars, have too much inertia to generate a time-efficient step-stare pattern. Our scheme uses a high-speed back-scanning MEMS correction mirror that will work in tandem with the primary scan mirror to keep the beam on target during the staring phase. Figures 2-4 detail this scheme. At the end of the staring phase, the combination of continuous

MOEMS and Miniaturized Systems XXI, edited by Hans Zappe, Wibool Piyawattanametha,
Yong-Hwa Park, Proc. of SPIE Vol. 12013, 120130B · © 2022 SPIE
0277-786X · doi: 10.1117/12.2610861

movement of the primary scan mirror and the rapid retrace of the correction mirror steps the beam to the new pointing direction. The increase in lidar signal amplitude and sensitivity enabled by step-stare can permit maximally sensitive detection while preserving the speed of the primary scan mirror.

The correction mirror can be fast partly because the required scan angle is small. The scan range of the correction mirror determines the size of the "step" for step-stare scanning and is related to the sparsity of data in the lidar point cloud. The mirror we describe here is capable of a scan range equivalent to 10 resolvable spots. Compared to slowly scanning and recording at a point density determined by the diffraction limited spot size, the step-stare system could scan ten times faster, recording 10 times fewer data points, but preserving maximal signal strength and range resolution for each point.

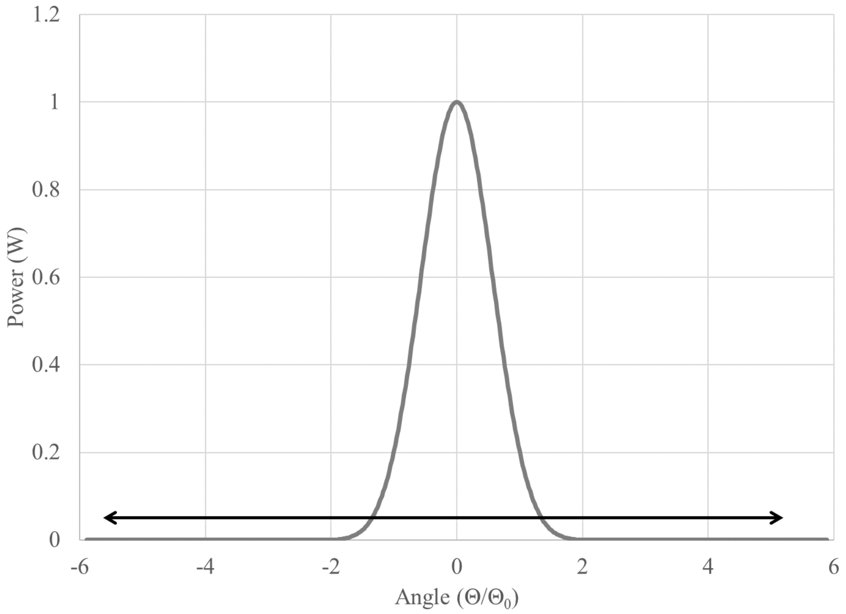

Figure 1. Coherent lidar normalized detected power vs. pointing angle for a point scatterer. In this example, the beam waist is located at the exit pupil, with pupil radius equal to 1.2 times the 1/e^2 intensity radius (beam waist radius), and the scatterer is in the far field. The scan angle is normalized to the Gaussian beam diffraction angle $\theta_0 = \lambda/\pi w_0$. The horizontal arrow indicates the full optical scan range of the MEMS correction mirror.

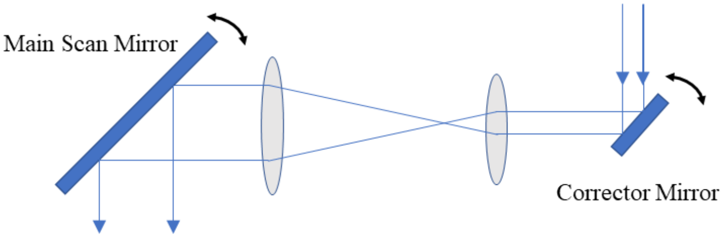

Figure 2. The mirror configuration for step-stare. The MEMS back-scanning corrector mirror has a small aperture, high bandwidth, and small stroke. The main scan mirror is a galvo with a large aperture, low bandwidth, and large angle of deflection. The MEMS corrector mirror compensates for the movement of the main scan mirror to hold the coherent lidar beam on target.

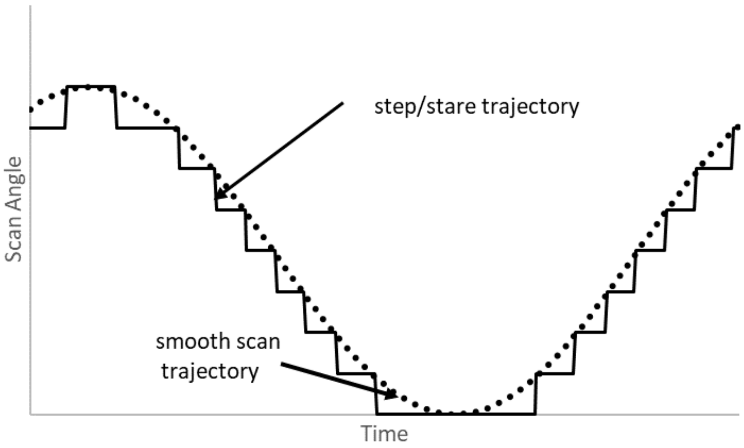

Figure 3. Trajectory over time for the step-stare configuration. The corrector mirror holds the beam on target while the angle of the main scan mirror changes continuously.

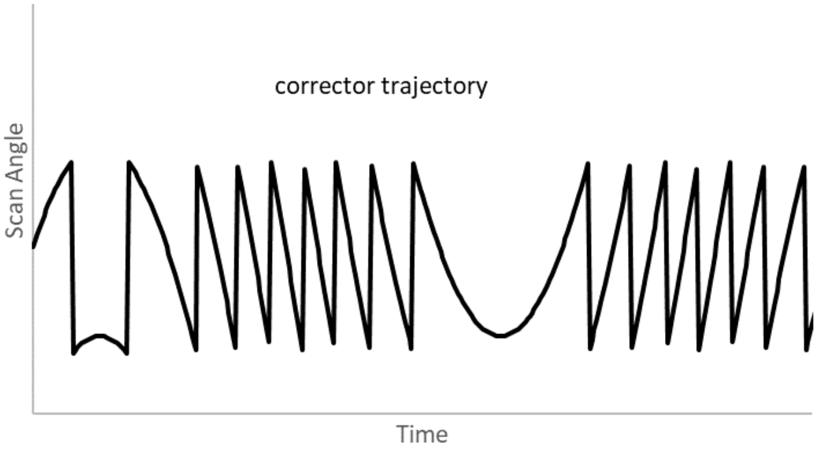

Figure 4. Trajectory of the MEMS corrector fast scan mirror. The overall trajectory of the optical system is shown in Figure 3.

3. PRIOR WORK

3.1 Step Stare

The step stare methodology has been used in imaging applications where a secondary back-scanning mirror is used to hold the image steady while either the primary scanner moves, or the entire system moves relative to the objects being imaged. For example, Chang[2] describes an implementation of step-stare with a fast scanning mirror mounted on voice coils to compensate for a rotating imaging platform. In the application described here, the back-scanning concept is adapted to a lidar, with a galvo mirror moving continuously, and the MEMS corrector mirror acting to hold the beam on target. We are unaware of prior work using MEMS backscanning for lidar beam pointing.

3.2 MEMS for lidar

MEMS mirrors for lidar applications are discussed by Holmström, Wang, and Raj[3-5]. Typically, MEMS mirrors used in lidar applications are primary scan mirrors, often with two axes of motion, and resonant in one or both axes. The review paper by Römer compares MEMS mirrors to electro-optic and acousto-optic deflectors[6]. The mirror we report has a higher bandwidth than other mirrors reported in the literature and is intended to operate as a broadband, non-resonant scanner with a deflection waveform that can be customized and varied (Figure 3 and Figure 4 illustrate a representative scan waveform). For this application, a large number of resolvable spots are not required and the mirror trades range of motion for a fast response. Also, a MEMS mirror is preferred to an acousto-optic modulator for chirped-pulse coherent lidar, because acousto-optic modulators shift the optical frequency of the pulse, affecting the lidar range information.

4. DESIGN

4.1 Design constraints

The design goal is a fast back-scanning correction mirror with a 10% step settling time of under 10 µs. The mirror should have a scan range of at least 10 resolvable spots at a wavelength of 780 nm, which necessitates an edge deflection of approximately ±1 µm. Furthermore, the drive voltage should be less than 400 V to reduce the system cost and ease integration. Challenges associated with these devices include obtaining a high resonant frequency with electrostatic actuation at a reasonable voltage, designing a mirror that does not distort under either electrostatic forces or inertial forces, and damping the movement of the mirror.

In the simplest terms, the resonant frequency of a MEMS mirror is given by Equation 1 where k_Θ is the torsional spring constant, and I is the mass moment of inertia.

$$f_r = \sqrt{k_\theta / I} \tag{1}$$

The spring constant for a rectangular cross-section rotating bar is

$$k_\theta = G\frac{ab^3}{L}\left(\frac{1}{3} - 0.21\frac{b}{a}\left(1 - \frac{b^4}{12a^4}\right)\right) \tag{2}$$

where G is the shear modulus, a and b are the cross sectional dimensions with $b \leq a$ and L is the length. This equation uses the notation of Kaajakari[7]. The spring constant is constrained because it must be low enough to allow the mirror to deflect at least 1 µm (static deflection at the mirror edge) at an applied voltage of 400 V. The mass moment of inertia for a disk of uniform thickness and density is given by Equation 3 where m is the mass, r is the radius, ρ is the mass density, and t is the mirror thickness.

$$I = \frac{1}{4}mr^2 = \frac{1}{4}\pi\rho t r^4 \tag{3}$$

Mirror radius has the greatest impact on the mass moment of inertia. Optical design considerations for the lidar favor a larger mirror, and we have selected $r = 1$ mm as an acceptable value for both mechanical performance and optical performance. The mass of the mirror is proportional to the thickness while the stiffness of the mirror is proportional to the cube of the thickness. The thickness $t = 300$ µm ensures that both static and dynamic mirror deflection remains below the diffraction limit.

The restriction on maximum applied voltage is a practical one rather than a restriction based on physics. The availability of high voltage amplifiers that operate above 400 V and at frequencies above 100 kHz is limited and the price increases as the voltage and frequency increases. The system integration issues of high voltage include breakdown in the air between the electrodes and the mirrors and the breakdown of the silicon dioxide between the electrodes and the grounded mirror wafer.

Because single crystal silicon has low mechanical losses, MEMS mirrors often have a high mechanical quality factor. For this design, damping is dominated by squeeze film damping in the gas surrounding the mirror. As will be discussed subsequently, these mirrors are underdamped at atmospheric pressure, with a quality factor in the range $10 < Q < 25$.

4.2 Finite Element Modeling

We verified our hand calculations by using finite element analysis. Specifically, we used the MEMS module of COMSOL version 5.6 from COMSOL AB[9]. We first used coupled electrostatic and mechanical analysis to determine the dimensions of the springs for an applied voltage of 400V and a maximum deflection of 1 µm. The analysis was iterative, and the software showed pull-in instability when the deflection exceeded about 35% of the 3 µm gap[8]. Once the dimensions were determined, the next step was mechanical simulation of eigenfrequencies and eigenmodes to determine the resonant frequency of the mirror. The dimensions were then iterated to obtain the maximum performance. We also analyzed the mirror flatness due to quasi-static electrostatic forces. For this we calculated the deflection of the mirror in COMSOL and had the software output an array of points reflecting the deflection of the surface. We then calculated the rms surface deviation from a plane and compared it to the Maréchal criterion which is λ/28 for a reflective surface. This set the minimum thickness of the mirrors to between 200 and 300 μm. We also calculated the impact of inertial forces on the mirror during switching and found the dynamic distortion to be much less than the quasi-static deflection due to the applied electrostatic force. Lastly, we calculated the impact of squeeze film damping by solving the modified Reynold's equation at mesh points on the underside of the mirror and converting the results into a force that opposes the motion of the mirror. This method is described by COMSOL[10] and by Bao[11]. A representative result of a simulation showing the relative motion of the mirror at the first resonant frequency is shown in Figure 5.

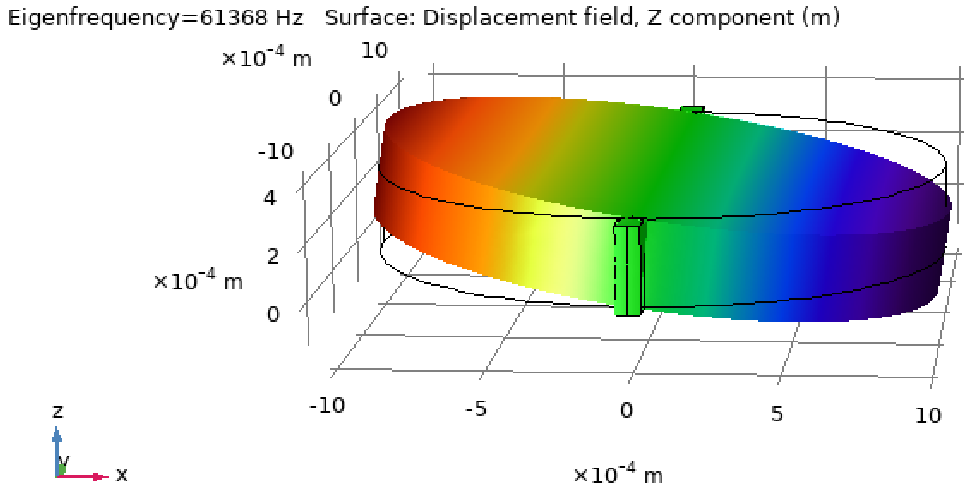

Figure 5. Graphical output of the COMSOL finite element tool showing a simulation of mirror movement at the first eigenfrequency.

5. FABRICATION

Prototype mirrors were fabricated in the Montana Microfabrication Facility at Montana State University. The starting material was <100> silicon wafers, 100 mm in diameter, and 300 μm thick, with a starting resistivity of 1-10 Ohm-cm. The backside of the silicon wafer was selectively recessed under the mirror by 3 μm to establish the air gap that permits mirror movement. Then, 1 μm of silicon dioxide was grown on the surface at 1050° C as an insulating layer. A gold layer was deposited onto the mirror to improve the reflectivity of the surface. An aluminum layer was used to make electrical contact to the silicon for electrostatic actuation. Separately, aluminum was deposited and patterned on a 1 mm thick borosilicate glass substrate to form electrodes. This borosilicate glass substrate was anodically bonded to the silicon substrate at 400° C and 800V for 25 minutes in an AML Aligner Wafer Bonder. The springs and mirror were then formed by etching through the wafer to the glass substrate using an inductively coupled plasma in an Oxford ICP etcher. The mirror surface of the bonded stack was protected by thermal release tape while the wafer was diced with a conventional dicing saw. Figure 6 shows a cross section of the device and Figure 7 shows the completed device as captured by a scanning electron microscope in the ICAL laboratory at Montana State University.

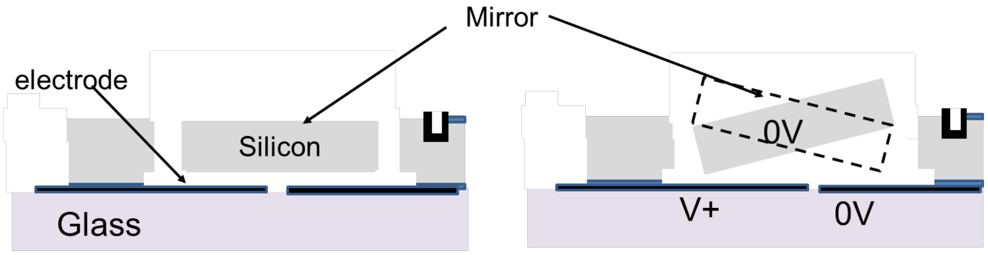

Figure 6. Cross section drawing of MEMS mirrors. The hinge supporting the mirrors is in the center of the mirror and is oriented out of the page.

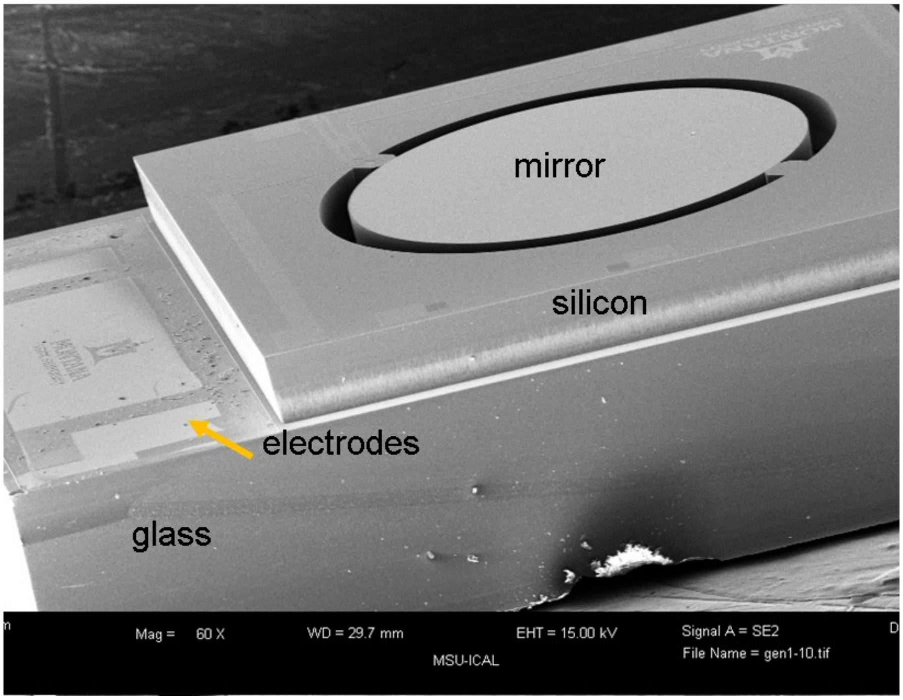

Figure 7. Scanning Electron Microscope (SEM) image of completed device. The glass substrate is 1 mm thick, and the silicon substrate, mirrors, and flexures are 300 μm thick.

6. TESTING AND EXPERIMENTAL RESULTS

6.1 Test Apparatus

The mirrors were actuated with a function generator or a dc power supply whose signal was amplified by a PZD 350 Piezo Driver amplifier manufactured by Trek Inc. A 10 kΩ resistor was placed between the mirror electrode and the amplifier to prevent damage to the mirror in case of short circuit. The deflection of the mirrors was measured optically by using a 12 mW, 633 nm He:Ne laser. The mirror deflection was calibrated by mounting it on a Picomotor stage from MKS. The deflection of the laser beam from the mirror was monitored with a Thor Labs PDA155 amplified silicon photodetector with a 50MHz bandwidth. Figure 8 shows the experimental setup.

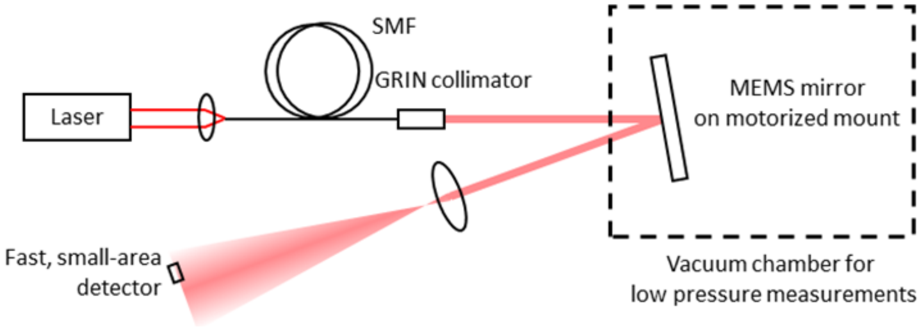

Figure 8. Drawing of characterization apparatus for the MEMS mirrors. The fiber and fiber collimator provide spatial filtering to improve the optical signal to noise ratio at the amplified silicon detector (Thor Labs PDA 155). A positive 50 mm focal length lens expands the beam relative to the 1 mm^2 silicon detector.

6.2 Frequency response

The displacement of the mirror was measured as a function of frequency. The driving signal was a sine wave with an offset that is half the peak to peak amplitude. The signal was generated by a function generator and then amplified. Because the mirror is a resonant structure, the driving voltage and offset were reduced as the device approached resonance to avoid causing the mirror to impact the electrodes. The experimental results are shown in Figure 9 and are normalized by the square of the applied voltage. A three factor Lorentzian fit, used to determine Q, is also included in Figure 9.

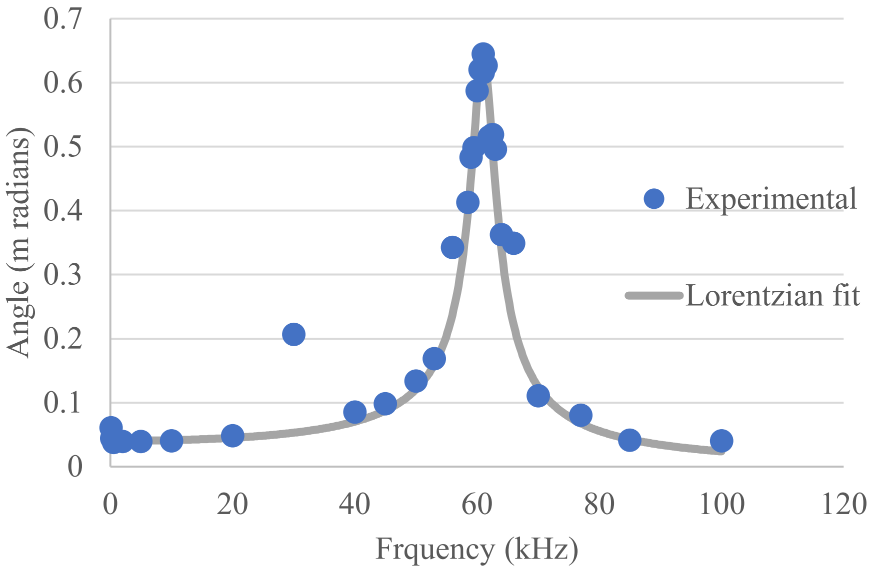

Figure 9. Response of mirror vs. frequency for a mirror operated at atmospheric pressure. The Lorentzian fit was used to determine Q. The peak at 30 kHz is due to a half frequency harmonic in the drive signal as described in Kaajakari[12].

To measure Q, a voltage step was applied to the mirror. Q was calculated in Equation 4 from the resonant frequency, f_0 and the time constant of the exponential decay, neper frequency, α. This was compared to the Q obtained from Lorentzian fits to the frequency response data. The results ranged from $100 < Q < 400$ in vacuum, and $10 < Q < 25$ in air at atmospheric pressure (Bozeman, MT, elevation ~ 5000 ft).

$$Q = \frac{1}{2*\alpha} * 2 * \pi * f_0 \tag{4}$$

6.3 Static Deformation

The static deformation of the mirror was measured by a Filmetrics 3D profilometer, a white light interferometer. For this measurement, the pixel size was 7 µm and the vertical resolution was 0.005 µm. The result was filtered by an 80 µm low pass filter to eliminate small scale defects. The result was a rms deviation value of 26 nm or less, which is λ/30 for a wavelength of 780 nm and is better than our λ/28 requirement. Figure 10 shows a screen shot of the unprocessed image. Note that the interferometer interprets metal lines on the surface of the silicon dioxide and the gold on the surface of the mirror as a step. The rms simulated value of the deformation using finite element analysis was 21 nm or λ/37 and is shown in Figure 11.

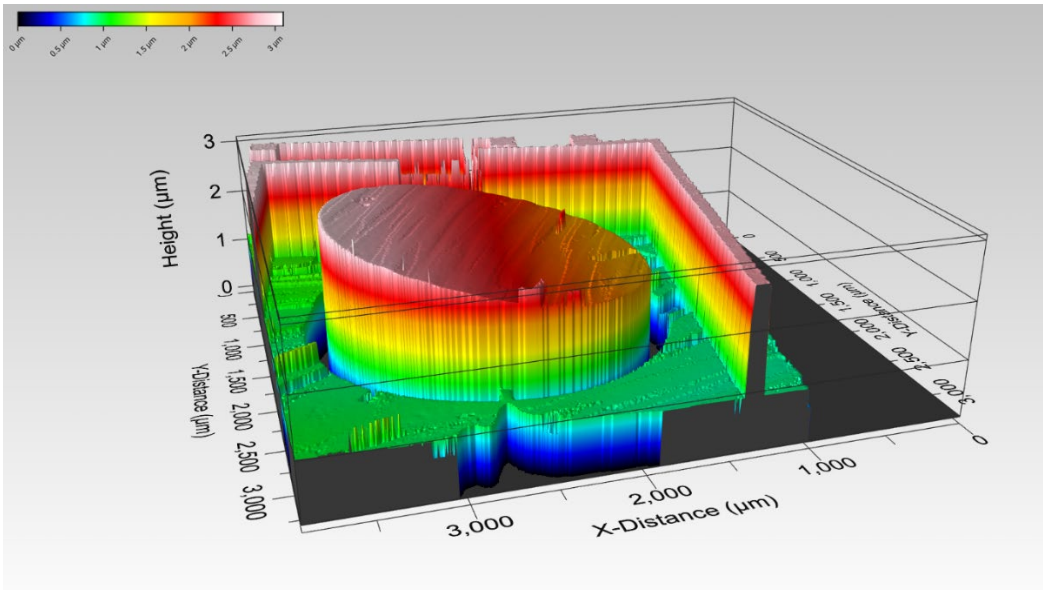

Figure 10. Output of Profilm 3D white light interferometer showing mirror being deflected 1 milliradian at an applied voltage of 405V. The mirror is coated with a layer of gold and there are aluminum interconnections on the mirror frame. The white light interferometer interprets these changes in reflection incorrectly as exaggerated changes in the "z" dimension.

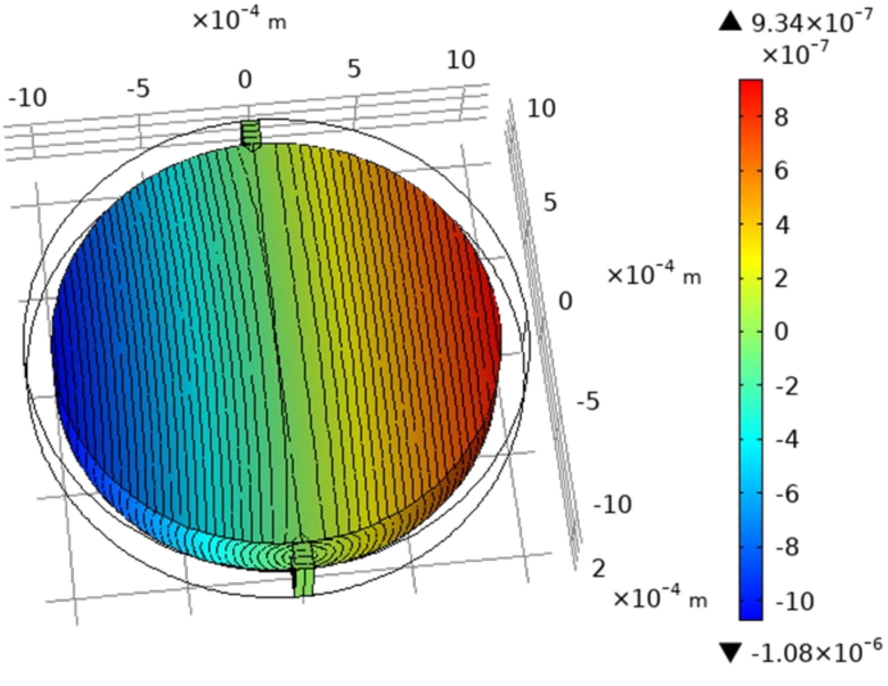

Figure 11. Simulation of deformation of MEMS mirror with 400 V applied to one electrode. The rms deformation from a plane was 21 nm and can be seen in the bending of the contour lines in the left part of the figure. The right side of the mirror is not being deformed downwards by electrostatic force and thus the contour lines are straight.

7. FUTURE WORK

Current efforts include inserting the mirror into a coherent lidar system to demonstrate the backscanning step-stare concept. We are developing a voltage actuation waveform tuned to reduce ringing when performing rapid re-trace using these underdamped mirrors. We are also developing designs to increase the resonant frequency of the devices, reduce the underdamped behavior as well as double the number of resolvable spots. Solutions to these challenges will concentrate on increasing the electrostatic force and reducing the mass of the mirror.

8. CONCLUSION

This paper reports a one axis non-resonant MEMS mirror for use as a secondary scan mirror to generate step-stare beam scan trajectories for coherent lidar applications. The prototype silicon mirror has a resonant frequency of 61 kHz, a diameter of 2 mm, a thickness of 300 µm, and achieves ten resolvable spots at a wavelength of 780 nm. Simulations and experiments indicate that the mirror should remain diffraction limited during static and high-speed scanning. Underdamped behavior with Q values ranging from 10 to 25 will require system-level tuning to achieve the target of 10% settling times that are less than 10 µs.

9. ACKNOWLEGDEMENTS

Photomasks were built at the Minnesota Nano Center, which is supported by the National Science Foundation through the National Nanotechnology Coordinated Infrastructure (NNCI) under Award Number ECCS-2025124. Fabrication work was performed, and images were taken at the Montana Nanotechnology Facility, a member of the National Nanotechnology Coordinated Infrastructure (NNCI), which is supported by the National Science Foundation (Grant# ECCS-2025391). Adam Eichhorn's internship at Montana State University was funded by the National Science Foundation under its Research Experience for Undergraduates program grant number 1949182. This project was funded by the Air Force Research Lab via a subcontract from S2 Corp. through award FA8650-16-C-1954 with a fundamental research exemption.

REFERENCES

[1] Oliver, A. and Dickensheets, D., "MEMS back-scanning mirrors for step-stare scanning for chirped pulse coherent lidar," 2021 IEEE Research and Applications of Photonics in Defense Conference (RAPID), 1-2, (2021).
[2] Chang, T., Wang, Q., Zhang, L., Hao, N., and Dai, W., "Battlefield dynamic scanning and staring imaging system based on fast scanning mirror," Journal of System Engineering and Electronics, 30(1), 37-56, (2019).
[3] Holmström, S., Baran, U., and Urey, H., "MEMS Laser Scanners: A. Review," Journal of Microelectromechanical Systems, 23(2), 259-274, (2014).
[4] Wang, D., Watkins, C., and Xie, H., "MEMS Mirrors for LiDAR: A. Review," Micromachines, 11(5), 456, (2020).
[5] Raj, T., Hashim, F., Huddin, A., Ibrahim, M. and Hassain, A., "A survey on lidar scanning mechanisms, Electronics, 9(5), 741, 2020.
[6] Römer, G. and Bechtold, P., "Electro-optic and acouto-optic laser beam scanners", Physics Procedia, 56 29-39, (2014).
[7] Kaajakari, V., [Practical MEMS], Small Gear Publishing, Las Vegas, 62-63 (2009).
[8] Moeenfard, H., and Ahmadian, M. "Analytical closed form model for static pull-in analysis in electrostatically actuated torsion micromirrors," Journal of Mechanical Science and Technology, 27(5), 1443-1449, (2013).
[9] https://www.comsol.com/comsol-multiphysics
[10] https://www.comsol.com/model/download/935521/models.mems.squeeze_film_perforated_plates.pdf, (3 January 2022).
[11] Bao, M. and Yang, H., "Squeeze film air damping in MEMS," Sensors and Actuators A, 136 3-27, (2007).
[12] Kaajakari, V., [Practical MEMS], Small Gear Publishing, Las Vegas, 223-236 (2009).